

The Role of Bi₂O₃ on the Thermal, Structural, and Optical Properties of Tungsten-Phosphate Glasses

Danilo Manzani,^{*,†} Cid B. de Araújo,[‡] Georges Boudebs,[§] Younès Messaddeq,^{†,||} and Sidney J. L. Ribeiro[†]

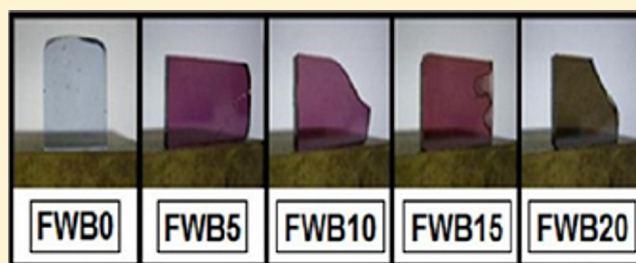
[†]Instituto of Chemistry, São Paulo State University, UNESP, CP 355, Araraquara, SP, 14801-970, Brazil

[‡]Departamento de Física, Universidade Federal de Pernambuco, 50670-901 Recife, PE, Brazil

[§]LUNAM Université, LPhiA, Laboratoire de Photoniques d'Angers, EA 4464, Université d'Angers, 2 Boulevard Lavoisier, 49045 Angers Cedex 01, France

^{||}Centre d'Optique, Photonique et Laser, Université Laval, 2375 Rue de la Terrasse, G1 V 0A6 Québec, Canada

ABSTRACT: Glasses in the ternary system (70 - x)NaPO₃-30WO₃- x Bi₂O₃, with $x = 0$ –30 mol %, were prepared by the conventional melt-quenching technique. X-ray diffraction (XRD) measurements were performed to confirm the noncrystalline nature of the samples. The influence of the Bi₂O₃ on the thermal, structural, and optical properties was investigated. Differential scanning calorimetry analysis showed that the glass transition temperature, T_g , increases from 405 to 440 °C for $0 \leq x \leq 15$ mol % and decreases to 417 °C for $x = 30$ mol %. The thermal stability against devitrification decreases from 156 to 67 °C with the increase of the Bi₂O₃ content. The structural modifications were studied by Raman scattering, showing a bismuth insertion into the phosphate chains by Bi–O–P linkage. Furthermore, up to 15 mol % of Bi₂O₃ formation of BiO₆ clusters is observed, associated with Bi–O–Bi linkage, resulting in a progressive break of the linear phosphate chains that leads to orthophosphate Q⁰ units. The linear refractive index, n_0 , was measured using the prism-coupler technique at 532, 633, and 1550 nm, whereas the nonlinear (NL) refractive index, n_2 was measured at 1064 nm using the Z-scan technique. Values of $1.58 \leq n_0 \leq 1.88$, $n_2 \geq 10^{-15}$ cm²/W and NL absorption coefficient, $\alpha_2 \leq 0.01$ cm/GW, were determined. The linear and NL refractive indices increase with the increase of the Bi₂O₃ concentration. The large values of n_0 and n_2 , as well as the very small α_2 , indicate that these materials have large potential for all-optical switching applications in the near-infrared.



1. INTRODUCTION

The development of nonlinear (NL) photonic devices is motivating the discovery of new optical glasses useful for all-optical switching, optical limiting, lasers, and infrared technologies. Among the glass families known chalcogenides^{1,2} and antimony based glasses^{3,4} are examples of materials having appropriate characteristics for photonic devices according to various authors. However, heavy-metal-oxides (HMO) such as Bi₂O₃, WO₃, Sb₂O₃, and PbO are subject of intense current research because their NL optical properties can be tailored using appropriate concentrations of elements with large hyperpolarizability and extended infrared transmittance.^{1,5–8} On the other hand, phosphate glasses, transparent from the ultraviolet to 5 μ m, have been increasingly applied in photonics due to their interesting properties, such as low glass transition temperature, T_g , and high thermal expansion coefficient that allows easy fabrication of optical fibers.^{9,10} Among the phosphate glasses, those based on sodium-polyphosphate are frequently used as host matrices because of their high vitrifying ability and unusual capability to dissolve large amounts of other glass formers, modifiers, or intermediate compounds without reduction of glass forming ability.¹¹ Several studies have shown that the physical properties and chemical durability of alkali-phosphate glasses can be improved by adding different metal

oxides of high valence cations like Al³⁺, Bi³⁺, Pb²⁺, W⁶⁺, Mo⁶⁺, etc., as these elements form relatively stable metal–O–P cross-linked bonds.^{12–14}

Moreover, HMO containing phosphate glasses have interesting physical properties and have been investigated in several studies.^{15–24} Montagne et al.¹⁵ studied the structure of ternary glasses P₂O₅–Bi₂O₃–Na₂O by ³¹P MAS NMR and infrared spectroscopy. Shaim et al.¹⁶ reported that the incorporation of BiO₆ and TiO₆ octahedrons into the glass structure results in the depolymerization of phosphate chains, leading primarily to pyrophosphate groups for low Bi₂O₃ content, whereas for high concentration of Bi₂O₃, orthophosphate groups become predominant as structural units. In addition, the optical properties of bismuth-phosphate glasses such as transmittance window and the NL optical susceptibility, $\chi^{(3)}$, also change with the presence of HMO inside the glass network. In particular, due to the large electronic densities and extended electronic clouds of the heavy atoms, an increase is observed in the NL refractive index, $n_2 \propto Re\chi^{(3)}$. Due to the same reason, glasses based on antimony, bismuth, tungsten, and

Received: October 1, 2012

Revised: December 4, 2012

Published: December 12, 2012

transition metals^{19–24} present large nonlinearity in the infrared. However, the choice of the appropriate material for all-optical switches is a challenge, because a high n_2 value is often accompanied by a large two-photon absorption coefficient, $\alpha_2 \propto \text{Im}\chi^{(3)}$, leading to reduction of the device performance. This behavior has motivated several groups to perform a characterization of different families of chalcogenide glasses owing to their large NL refractive index. Unfortunately most of chalcogenide glasses that have large n_2 for excitation near the band gap present poor figure-of-merit, $n_2/\lambda\alpha_2$, for all-optical switching.²⁵

NL optical absorption studies on $\text{NaPO}_3\text{--BaF}_2\text{--WO}_3$ glass system, have shown that samples with more than 40% of WO_3 molar content in the glass composition, have potential as optical limiters due to the high polarizability of tungsten oxide clusters formed up to this WO_3 concentration, which increase the NL optical parameters.²⁴ Also binary compositions of tungsten-lead-pyrophosphate glasses ($\text{Pb}_2\text{P}_2\text{O}_7\text{--WO}_3$) were studied in the near-infrared region, and the results have shown that their NL response is faster than 100 fs and that an increase of n_2 occurs with the increasing of the WO_3 amount in the samples.²³

Bismuth-based glasses are also promising materials since they present large NL properties.^{26,27} Conventional network formers such as P_2O_5 and SiO_2 containing a high concentration of Bi_2O_3 attract much attention for optical transmission applications,²⁸ and their high nonlinearity indicates that the Bi-based glasses are useful for ultrafast optical switches.

Motivated by our previous results with the tungstate-phosphate glass²³ we performed a detailed study of the Bi_2O_3 influence on the physical properties of the glass system $\text{NaPO}_3\text{--WO}_3\text{--Bi}_2\text{O}_3$. Thermal, structural, and optical properties were investigated as a function of the glass composition applying the techniques of differential scanning calorimetry (DSC), X-ray diffraction (XRD), Raman spectroscopy, linear absorption, and linear refractive index measurements as well as NL optical techniques. The figure of merit $n_2/\lambda\alpha_2$ for all-optical switching was determined using the NL parameters measured, and the results indicate a large potential of the $\text{NaPO}_3\text{--WO}_3\text{--Bi}_2\text{O}_3$ composition for photonic devices in the near-infrared region.

2. EXPERIMENTAL SECTION

2.1. Glass Preparation. Glass samples were prepared by melting the raw materials sodium metaphosphate NaPO_3 (99+ % pure), tungsten oxide WO_3 (99.8% pure) and bismuth oxide Bi_2O_3 (99.8% pure) previously stoichiometrically weighted, with the compositions $(70 - x)\text{NaPO}_3\text{--}30\text{WO}_3\text{--}x\text{Bi}_2\text{O}_3$ for $x = 0, 5, 10, 15, 20, 25$, and 30 mol %. First, the raw materials were mixed and heated at 400 °C for 1 h to remove water and adsorbed gases. Then, the batch was melted at a temperature ranging from 950 to 1100 °C, depending on the Bi_2O_3 content, during 40 min to ensure homogenization and fining. Finally, the melt was cooled inside a metal mold preheated to 20 °C below the glass transition temperature, T_g , and then, annealing was implemented at this temperature for 2 h in order to minimize mechanical stress resulting from thermal gradients upon cooling.

The WO_3 concentration was fixed at 30 mol % for all samples, based on previous studies that showed an increasing of the network stability with tungsten oxide insertion. Above this concentration the formation of WO_n polyhedral clusters is observed being mainly characterized through the W–O–W

bond stretch band in the Raman spectra. These structural features lead to an increase of the linear and NL refractive indices owing to the high electronic polarizability of the W-based polyhedrons.²⁴

2.2. Glass Characterization. Characteristics temperatures (T_g for glass transition, T_x for onset of crystallization, and T_p for maximum of crystallization peak) were determined by DSC. The estimated error in the temperatures measurements is ± 3 °C for T_g and T_x (obtained from tangents intersection) and ± 1 °C for T_p . Powdered samples with granulometry of $0.063 < x < 0.102$ mm were set in aluminum pans under N_2 atmosphere and a heating rate of 10 °C/min was used for the DSC analysis. Raman scattering spectra were recorded at room temperature in the frequency range from 100 to 1300 cm^{-1} by using a HORIBA Jobin Yvon model LabRAM HR micro Raman apparatus equipped with a 632.8 nm laser delivering 30 mW power. UV–visible absorption spectra and infrared transmittance of the glasses samples were recorded from 200 to 2000 nm with a Varian Cary 500 spectrophotometer, and from 400 to 4000 cm^{-1} using a Perkin-Elmer FT-IR Spectrum 2000. Refractive indices were measured at three wavelengths (532, 632.8, and 1550 nm) by the prism-coupler technique with a Metricon-2010 instrument. Finally, the NL susceptibility of the samples was investigated applying the Z-scan technique^{29,30} using the setup shown in Figure 1. The excitation is provided

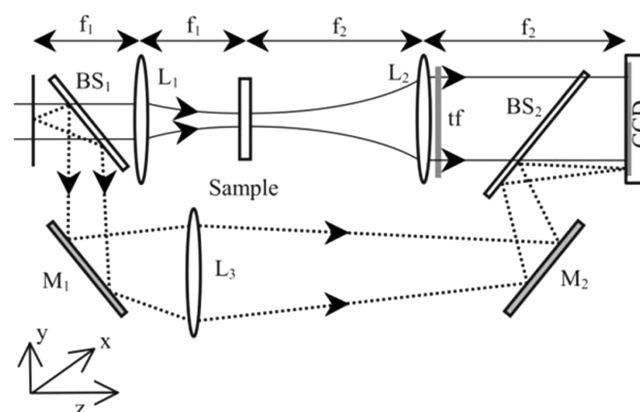


Figure 1. Experimental Z-scan setup. The labels refer to lenses (L_1 and L_2), mirrors (M_1 and M_2), beam splitters (BS_1 and BS_2), and neutral filters (tf). The sample is moved in the focal region between L_1 and L_2 .

by a linearly polarized Nd:YAG laser (1064 nm, pulses of 17 ps and repetition rate of 10 Hz). The measurements were performed with incident intensities on the samples varying from 3 to 35 GW/cm^2 . For calibration we used CS_2 as a reference sample considering $n_2 = 3.0 \times 10^{-18} \text{ m}^2/\text{W}$.²⁹ The image receiver is a 1000×1800 pixels charge coupled device (CCD) cooled camera operating at -30 °C with a field gain.

A reference beam incident on a small area of the camera allows monitoring the energy fluctuation of the laser pulses to take into account the intensity changes in the calculation of the NL parameters. The samples are scanned in the focus region along the beam propagation direction (z axis) as in the original Z-scan setup.²⁹ Open aperture and closed aperture normalized transmittances were numerically processed from the acquired CCD images by integrating over all camera pixels in the first case and over a circular numerical filter in the second case (corresponding to a linear aperture transmittance $S = 0.4$). Equation 13 of ref 29 relating the NL parameters to ΔT_{p-v} the

difference between the normalized peak and valley transmittances in the Z-scan profile, remains valid for the 4f system used here.

3. RESULTS

The glasses prepared in the ternary system $\text{NaPO}_3\text{--WO}_3\text{--Bi}_2\text{O}_3$ are reasonably transparent and their colors vary from purple to brown with increase of the Bi_2O_3 concentration as shown in Figure 2. The samples were optically homogeneous to naked eyes and free of strains due to the high melt temperatures, large melting time, and low cooling rates used.

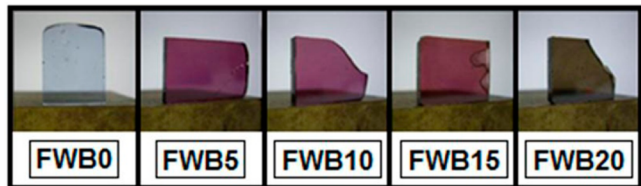


Figure 2. Picture of glass samples in the ternary system $\text{NaPO}_3\text{--WO}_3\text{--Bi}_2\text{O}_3$.

The typical noncrystalline halo was observed in X-ray diffraction for all compositions, as shown in Figure 3. The samples containing 25 and 30 mol % of Bi_2O_3 were not obtained as bulk samples due to their low thermal stability.

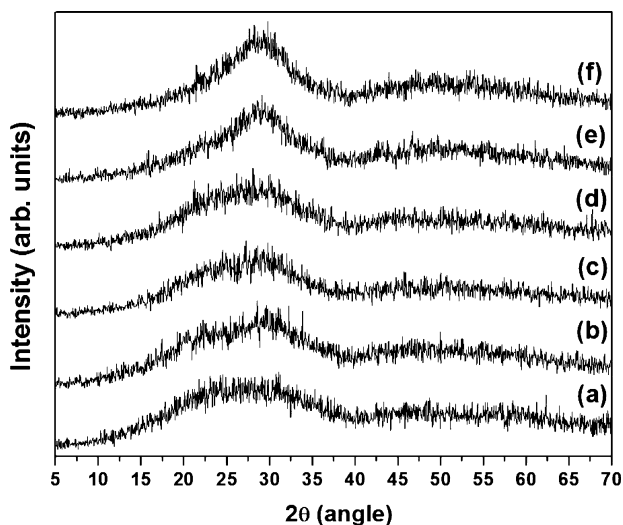


Figure 3. X-ray diffraction of the FWB glass samples (a) FWB5, (b) FWB10, (c) FWB15, (d) FWB20, (e) FWB25, and (f) FWB30.

Table 1 shows values obtained for the characteristics temperatures. Increasing the Bi_2O_3 content, the value of T_g increases up to 15 mol % (FWB15). Above that Bi^{3+} content a decrease in T_g was observed. Thermal stability against crystallization was evaluated with the thermal stability parameter $\Delta T = T_x - T_g$ and the addition of bismuth oxide in the glass matrix leads to a decrease of ΔT .

Raman spectra for all samples and reference compounds are shown in Figure 4, and the band assignments are shown in Table 2. Sodium metaphosphate is constituted by linear chains of $[\text{PO}_4]$ tetrahedrons and the Raman spectra present two strong bands at ~ 710 and $\sim 1160 \text{ cm}^{-1}$ assigned to symmetric stretching of P–O–P linkage and symmetric terminal stretching of P–O bonds of metaphosphate (Q^2) tetrahedrons,

Table 1. Molar Compositions and Characteristics Temperatures of the $(70 - x)\text{NaPO}_3\text{--}30\text{WO}_3\text{--}x\text{Bi}_2\text{O}_3$ Glasses

samples labels	molar compositions (%)		characteristics temperatures ($^{\circ}\text{C}$)	
	NaPO_3	Bi_2O_3	T_g	T_x
FWB0	70	0	405	
FWB5	65	5	414	571
FWB10	60	10	433	550
FWB15	55	15	440	530
FWB20	50	20	432	513
FWB25 ^a	45	25	421	496
FWB30 ^a	40	30	417	484

^aNot obtained as bulk samples.

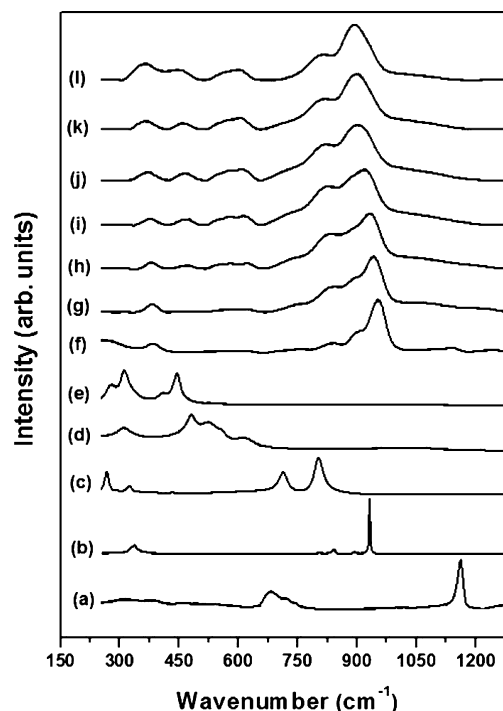


Figure 4. Raman spectra of the glass samples in the ternary system $\text{NaPO}_3\text{--WO}_3\text{--Bi}_2\text{O}_3$ and reference compounds: (a) NaPO_3 , (b) NaWO_4 , (c) WO_3 , (d) NaBiO_3 , (e) Bi_2O_3 , (f) FWB0, (g) FWB5, (h) FWB10, (i) FWB15, (j) FWB20, (k) FWB25, and (l) FWB30.

respectively.³¹ Two weak bands centered at ~ 1010 and $\sim 1270 \text{ cm}^{-1}$ are assigned to symmetric terminal stretching of P–O bonds of pyrophosphate (Q^1) tetrahedrons and asymmetric stretching of P–O bonds of Q^2 units, respectively. The very weak broad band observed at 330 cm^{-1} refers to deformation stretching of the PO_4 tetrahedra.³²

Monoclinic WO_3 is constituted of distorted WO_6 octahedrons where all the corners are shared building up a tridimensional crystalline network. Two bands at ~ 810 and $\sim 720 \text{ cm}^{-1}$ are assigned to asymmetric and symmetric stretching vibrations of W–O–W linkages, respectively. The two weak shoulders at ~ 330 and $\sim 280 \text{ cm}^{-1}$ are assigned to bending vibrations of WO_6 octahedrons and the bands at ~ 930 and $\sim 810 \text{ cm}^{-1}$, observed in Na_2WO_4 , are assigned to asymmetric and symmetric stretching vibrations of terminal W–O bonds.^{19,33,34}

Similarly to the tungsten oxide structure, Bi_2O_3 is also constituted by highly distorted BiO_6 octahedrons with all corners shared, presenting four bands at ~ 280 , ~ 310 , ~ 410 ,

Table 2. Raman Assignments for Reference Compounds and the FWB Glasses^a

NaPO ₃	WO ₃	Na ₂ WO ₄	Bi ₂ O ₃	NaBiO ₃	FWB glasses
710 ν_s WOW	810 ν_s WOW	930 ν_{as} WO	280 ν_{as} BiOBi	480–550 ν_s and ν_{as}	~910
1160 ν_s (PO ₂ -Q ²)	720 ν_s WOW	810 ν_s WO ν_s WOW	310 ν_{as} BiOBi	BiO/Bi=O	~820
330 δ PO ₄	320 δ WO ₆	350 δ WO ₆	410 ν_s BiO (BiO ₆)	615 ν_s and ν_{as} BiO (BiO ₆)	~730
	275 δ WO ₆		450 ν_s BiO(BiO ₆)		~580
					~460
					~360

^aThe Raman shifts are in cm⁻¹.

and ~445 cm⁻¹ assigned to overlapping of asymmetric and symmetric stretching vibrations of Bi–O–Bi and Bi–O linkages of BiO₆ octahedron, respectively.³⁵ Raman bands at ~480, ~520, and ~553 cm⁻¹ observed in NaBiO₃ spectra (trigonal planar structure) are assigned to stretching vibrations of Bi–O and Bi=O terminal bonds; and the band located at ~615 cm⁻¹ is assigned to overlapping asymmetric and symmetric stretching vibrations of Bi–O of BiO₆ octahedron.³⁶

The Raman spectra of the NaPO₃–WO₃–Bi₂O₃ system exhibit characteristic features that can be used to monitor the structural dependence with the composition. The large band at ~910 cm⁻¹ attributed to P–O bonds of tetrahedral orthophosphate (Q⁰), progressively increased with increasing of the Bi₂O₃ content and is overlapped with the stretching vibrational mode of WO_n polyhedrons that remains intensity constant for all absorption bands centered at ~910, ~820, and ~360 cm⁻¹. The progressive BiO_n polyhedral insertion into the phosphate chains is evidenced by the increase of the bands at ~460 and ~580 cm⁻¹, assigned to vibration stretching of Bi–O linkages.

The glass transmittance is limited by the optical band gap in the ultraviolet–visible range and by the multiphonon absorption in the near- and middle-infrared. Figure 5a shows the absorption spectra of the samples from ~350 nm to ~800 nm, at room temperature. The addition of Bi₂O₃ shifts the band edge to larger wavelengths from ~362 nm for FWB0 to 400 nm for FWB20, as shown in the inset of Figure 5a. In Figure 5b the near-IR transmittance spectra of the FWB glass family are shown, and as seen in Figure 5a,b the samples have wide transmittance windows from ~375 to ~2950 nm that are characteristic of phosphate glasses.

The linear refractive indices were measured for all samples, and the results are indicated in Figure 6. It is noticeable that the FWB glasses exhibit a significant high refractive index compared with other phosphate glasses compositions.

The third-order optical nonlinearity of FWB glasses was measured with the Z-scan technique using a 17 ps Nd: YAG laser at 1064 nm. Figure 7 shows the transmittance change in the Z-scan profiles (closed aperture) for three representative samples, FWB5, FWB10 and FWB15. The experiments with the other samples show analogous behavior and similar signal-to-noise ratios. The NL refractive indices can be determined from the transmittance change (peak-to-valley), ΔT_{pv} , when the glass sample passes the focal point ($z = 0$). According to²⁹ the transmittance is described as $T = 1 - ((az)/((z^2 + 9)(z^2 + 1)))$, where a is determined experimentally ΔT_{pv} . For all samples the closed aperture Z-scan profiles indicate positive values of n_2 . The open aperture measurements did not show changes in the samples' transmittance and we concluded that α_2 is smaller than the detection limit of our apparatus (0.01 cm/GW). Calculations of n_2 for all samples were made following the procedure of ref 29 and the results are given in Figure 6. The

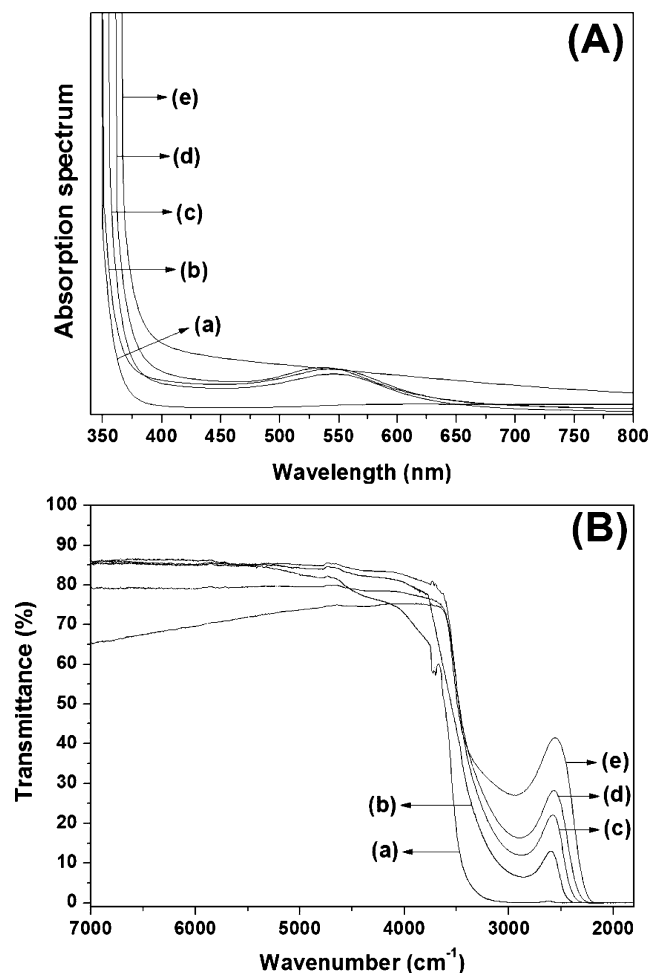


Figure 5. Linear absorption spectra (A) and infrared transmittance spectra (B) of the glass samples (a) FWB0, (b) FWB5, (c) FWB10, (d) FWB15, and (e) FWB20.

positive n_2 values are typically 1 order of magnitude larger than for silica.³⁷

4. DISCUSSIONS

Figure 8 exhibits the evolution of T_g and $(T_x - T_g)$ for Bi₂O₃ concentrations varying from 0 to 30 mol %. One interesting result is the anomalous behavior of T_g that increases up to Bi₂O₃ concentration of ~15% and decreases for larger concentrations. These results suggest that, initially, the inclusion of bismuth oxide into the glass increases the network connectivity (increasing the T_g), making them more rigid up to 15 mol % of Bi₂O₃, despite the continuous decrease of ΔT ; this means that the addition of bismuth atoms enhances the covalent character of the glass network. Similar behavior was

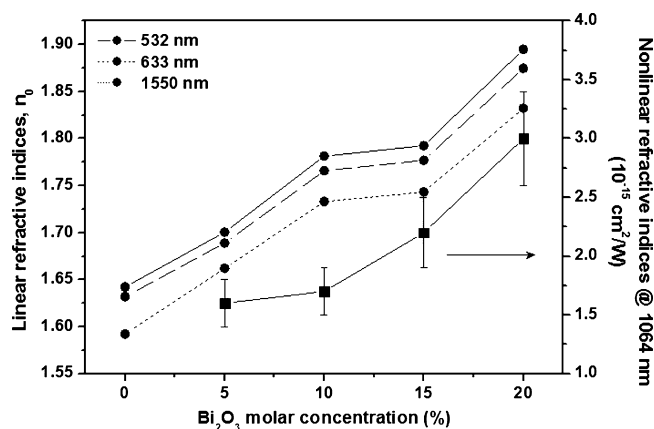


Figure 6. Linear refractive index (sphere-lines) and NL refractive index (square-line) behavior as a function of Bi₂O₃ molar concentration.

already demonstrated in other tungsten-phosphate glasses, varying WO₃ concentration instead of Bi₂O₃, and it was related with the increase of the network connectivity due to tungsten octahedrons insertion in the phosphate chains.¹⁹

On the other hand, for the samples with up to 15 mol % of Bi₂O₃, the bismuth atoms leads to depolymerization of the phosphate network due to the presence of BiO₆ octahedrons into the phosphate chains. The depolymerization process is reflected in the decrease of T_g from 440 to 417 °C. In fact, previous structural studies of glasses with high concentration of tungsten oxide (40 mol %) revealed decrease of the T_g owing to the presence of WO₆ octahedron clusters that lead to breaking the phosphate network.³⁸ Considering that the BiO₆ octahedrons are more bulky than WO₆ units, we conclude that the Bi₂O₃ incorporation above 15 mol % results in the glass network opening.

The thermal stability against crystallization was evaluated on the basis of the $\Delta T = T_x - T_g$ parameter. The results shown in Figure 8 indicate that the addition of bismuth oxide in the glass matrix leads to a decrease of ΔT , which ranges from 156 to 67 °C. This behavior may be related to the breaking of polyphosphate chains up to the FWB15 sample, generating small chains and resulting in lower viscosity above T_g . Consequently, there is an increase of the crystallization tendency of the glass system up to 15 mol % of Bi₂O₃. This behavior is consistent with a decreased network connectivity and lower viscosity above T_g , which is known to make more easy the structural reorganization and crystallization.³⁹

We remark that the structural investigations performed by Raman scattering showed an interesting modification in the vitreous network as a function of the Bi₂O₃ concentration. For samples with low concentration, the basic structure of the glasses can be described as a random pyrophosphate network. With the addition of bismuth oxide, BiO₆ octahedrons groups enter into the linear phosphate chains, creating PO₄³⁻ units and nonbridged oxygen W–O⁻ and Bi–O⁻. The presence of these bonds is confirmed by the stretching bands at ~600 and ~910 cm⁻¹, as shown in Figure 4. Therefore, the incorporation of Bi₂O₃ leads to a partial break of the linear pyrophosphate chains (Q¹) and the probable creation of orthophosphate isolated tetrahedral (Q⁰). This is evidenced by the progressive intensity increasing of the band centered at 900 cm⁻¹, which is overlapped with the bands at ~920 and ~810 cm⁻¹, assigned to vibrational stretching of W–O and W=O terminal bonds

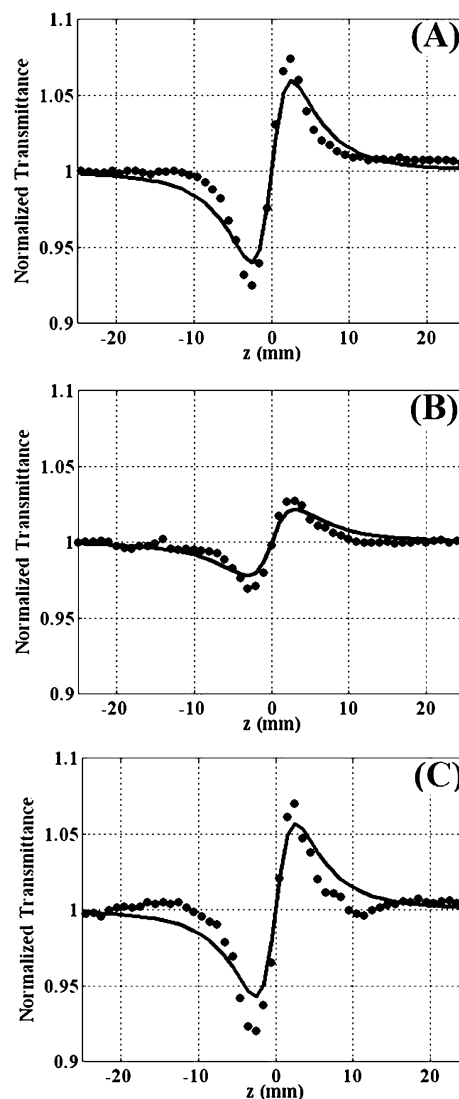


Figure 7. Closed-aperture Z-scan transmittances at 1064 nm. Experimental results (points) and theoretical fits (solid lines) for samples: (A) FWB5 (thickness of 1.23 mm and $I_0 = 36$ GW/cm²); (B) FWB15 (thickness: 1.72 mm; $I_0 = 20$ W/cm²); (C) FWB10 (thickness: 2.30 mm; $I_0 = 4.5$ GW/cm²). I_0 is the on-axis peak intensity at the focus of lens L_1 of Figure 1.

and W–O–W linkage of the WO_n polyhedrons. As reported for NaPO₃–BaF₂ glass system in ref 19 above 30 mol % of WO₃, clustering of WO_n polyhedral occurred as suggested by the observation of the Raman band at ~810 cm⁻¹. Important consequences of the presence of those structural units would be the increased connectivity of the phosphate network and enhanced NL properties. Also the progressive formation of orthophosphate groups directly reflects in the decreasing behavior of thermal stability, as discussed above.

Interestingly, the weak and broad Raman band centered at ~730 cm⁻¹ assigned to vibrational stretching of P–O–P linkage of pyrophosphate Q² tetrahedron, can be observed for samples with up to 25 mol % of Bi₂O₃. However, the Bi₂O₃ addition leads to breakdown of phosphate linear chains, followed by the observation of orthophosphate units, at the expense of pyrophosphate Q² units. So in this case, the anomalous behavior of T_g as a function of the Bi₂O₃ content, which is evident up to FWB25 sample, can be explained by the

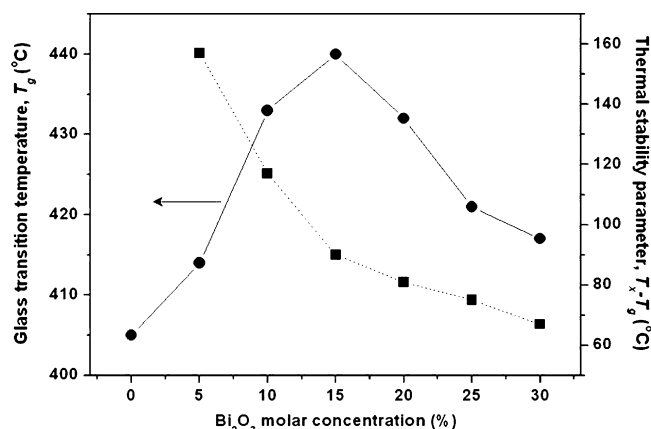


Figure 8. Behavior of the glass transition temperature (solid line) and the thermal stability parameter $T_x - T_g$ (dot line) as function of Bi_2O_3 concentration.

formation of P–O–Bi and also P–O–W bridge bonds, that contribute to the growth of T_g when x increases from 0 to 15 mol %.

Note that the WO_3 concentration remains constant at 30 mol % for all samples and no important intensity variation is observed for the Raman bands related to WO_6 octahedron. However, the energy shift of the Raman bands ($940\text{ cm}^{-1} \rightarrow 890\text{ cm}^{-1}$ and $835\text{ cm}^{-1} \rightarrow 812\text{ cm}^{-1}$) must be due to the change of the $[\text{WO}_6]$ chemical environment occurring with the addition of Bi atoms in the glass network.

The progressive BiO_n polyhedrons addition into the phosphate chains is also evidenced by the increase of the broad band centered at $\sim 580\text{ cm}^{-1}$ assigned to vibrational stretching of the terminal bonds Bi–O and Bi=O, that is due to the overlapping of the bands at ~ 460 and $\sim 610\text{ cm}^{-1}$ assigned to Bi–O bonds of the BiO_6 octahedron. The band centered at $\sim 360\text{ cm}^{-1}$ have a small intensity increase with the Bi_2O_3 concentration above 15 mol %, due to the vibrational stretching of Bi–O–Bi linkage of BiO_6 octahedrons. This behavior suggests clustering of BiO_n polyhedra with covalent bonds between the phosphate chains (Note that this band is overlapped with deformed WO_6 polyhedrons bands at ~ 330 and 280 cm^{-1}). This fact reflects in the T_g decrease when the Bi_2O_3 concentration is increased up to 15 mol % owing to the breakdown of the phosphate linear chains and P–O–Bi to form BiO_n polyhedrons clusters.

However, as shown in the Raman spectra, Q^0 tetrahedrons are not isolated units but have their oxygen atoms linked with bismuth atoms by P–O–Bi linkages. Thus, bismuth oxide acts breaking and modifying the linear phosphate of PO_4 tetrahedron and it is probably inserted between them to form a mixed chain of $\text{PO}_4\text{--BiO}_n$.

Figure 5 show that the increase of Bi_2O_3 concentration in the $\text{NaPO}_3\text{--WO}_3$ glass matrix originates shifts of the absorption spectrum to longer wavelengths corresponding to a decrease of the optical band gap. This behavior can be explained by the formation of a more covalent network suggested by the Raman results that is attributed to the insertion of BiO_n polyhedrons which links PO_4 units with highly covalent P–O–Bi, P–O–W and Bi–O–Bi bonds.

Furthermore, the samples FWB5, FWB10, and FWB15 show a large absorption band centered at $\sim 550\text{ nm}$ related to different oxidation states of tungsten and bismuth atoms, as well as localized defects around tungsten ions, as anion vacancy

in the polyhedrons or electrons trapped into the network defects, caused by the bismuth atoms insertion into the glass network. In addition, this absorption band is probably related to electronic d–d transitions of W^{5+} and/or W^{4+} reduced species and, as well as a redox equilibrium between reduced tungsten and oxidized bismuth species. W^{6+} ions do not absorb in the ultraviolet–visible range due to its electronic configuration $5d^0$.

Concerning the infrared transmission spectra of the glass samples shown in Figure 5 we notice that the glasses are transparent up to $\sim 2600\text{ cm}^{-1}$ ($\sim 3.8\text{ }\mu\text{m}$), that is characteristic of phosphate glasses, attributed to the third-harmonic vibration of the maximum vibration energy of P–O bond in PO_4 tetrahedrons.³⁹ The absorption band centered at $\sim 3000\text{ cm}^{-1}$ ($\sim 3.3\text{ }\mu\text{m}$), whose intensity decrease with Bi_2O_3 content, is attributed to P–O–H bonds present in the glasses, because all OH bonded with phosphorus were not eliminated during the synthesis.³⁹ The amplitude of this band slightly decreases with Bi_2O_3 content, which is consistent with larger chemical stability and less hygroscopic glasses due to a decrease of the phosphate content.

Figure 6 shows an increase of n_0 with respect to Bi_2O_3 concentration. This behavior can be understood considering that the BiO_n units are more polarizable than WO_n and PO_4 units, due to extended electron cloud in bismuth atoms. In addition, the refractive index increase is related with the progressive formation of BiO_n clusters (and WO_n clusters) that are much more polarizable than isolated BiO_n polyhedrons. This explains the large values of n_0 that are unusual in phosphate-based glasses and justify the investigation of the NL optical properties.

Examining Figure 7 it can be verified that both constituents WO_3 and Bi_2O_3 contribute for n_2 . The contribution of WO_3 for the NL response is attributed to the polarizability associated with the W–O bonds in WO_n clusters,⁴⁰ whereas the contribution of Bi_2O_3 is due to the large polarizability of the Bi–O–Bi bonds²¹ and it increases with the concentration of Bi_2O_3 . Using the results of the NL experiments, it was also calculated the figure-of-merit for all-optical switching $T = 2\lambda\alpha_2/n_2$. Values of $T < 0.7$ were obtained in the picosecond regime at 1064 nm indicating that $\text{NaPO}_3\text{--WO}_3\text{--Bi}_2\text{O}_3$ glasses can be used in devices such as directional couplers and NL distributed feedback gratings that require $T < 1$ and $T < 4$, respectively.⁴¹

5. CONCLUSIONS

Optical, structural and thermal investigations were performed on the $\text{NaPO}_3\text{--WO}_3\text{--Bi}_2\text{O}_3$ system using various techniques in order to understand the vitreous network and the dependence of the optical properties as a function of the relative amount of Bi_2O_3 in the glass composition. The $\text{NaPO}_3\text{--WO}_3\text{--Bi}_2\text{O}_3$ glass family presents good thermal stability against devitrification, high linear and NL refractive index and large transparency from 375 to 2950 nm. The Raman scattering results pointed out that the introduction of Bi_2O_3 depolymerizes the linear phosphate chains and results in the formation of P–O–Bi bonds that increase the network connectivity up to 15 mol % of Bi_2O_3 . In addition, the increase of Bi–O–Bi bonds in the samples containing more than 15 mol % of Bi_2O_3 with the formation of BiO_6 clusters, is reflected in high values of n_0 and, consequently, large n_2 . The results indicate that $\text{NaPO}_3\text{--WO}_3\text{--Bi}_2\text{O}_3$ glasses are good candidates for all-optical switching devices in the near-infrared thanks to

the addition of appropriate amount of bismuth oxide to the tungsten-phosphate glasses.

In summary, the large transmittance window, large linear and NL refractive index, as well as low NL absorption coefficient of the glass samples studied demonstrate their high potential for photonic applications. Moreover, according to the evolution of the thermal properties of this glass family, these materials can be used to fabricate optical fibers from preforms having the compositions reported here. Fibers with good optical quality are already being studied and their fabrication and characterization will be reported in the near future.

AUTHOR INFORMATION

Corresponding Author

*E-mail: danilo.manzani@gmail.com.

Notes

The authors declare no competing financial interest.

ACKNOWLEDGMENTS

We thank the Conselho Nacional de Desenvolvimento Científico e Tecnológico (CNPq) for financial support through the National Institute of Science and Technology of Photonics (INCT project). Support from the Fundação de Amparo à Pesquisa do Estado de São Paulo (FAPESP) and Fundação de Amparo a Ciência e Tecnologia do Estado de Pernambuco (FACEPE) is also acknowledged.

REFERENCES

- (1) El-Mallawany, R. A. H. *Tellurite Glasses Handbook: Physical Properties and Data*; CRC: Boca Raton, FL, 2002.
- (2) Zakery, A.; Elliott, S. R. *Optical Nonlinearities in Chalcogenide Glasses and their Applications*; Springer: Berlin, Germany, 2007.
- (3) Falcão-Filho, E. L.; de Araújo, C. B.; Bosco, C. A. C.; Maciel, G. S.; Acioli, L. H. *J. Appl. Phys.* **2005**, *97*, 013505–013505/5 and references therein..
- (4) Gómez, L. A.; de Araújo, C. B.; Putvinskis, R.; Messaddeq, S. H.; Ledemi, Y.; Messaddeq, Y. *Appl. Phys. B: Lasers Opt.* **2009**, *94*, 499–502 and references therein..
- (5) Yamane, M.; Asahara, Y. *Glasses for Photonics*; Cambridge University Press: Cambridge, U.K., 2000.
- (6) Sugimoto, N.; Kanbara, H.; Fujiwara, S.; Tanaka, K.; Shimizugawa, Y.; Hirao, K. *J. Opt. Soc. Am. B* **1999**, *16*, 1904–1908.
- (7) Smolorz, S.; Kang, I.; Wise, F.; Aitken, B. G.; Borrelli, N. F. *J. Non-Cryst. Solids* **1999**, *256&257*, 310–317.
- (8) Sekhar, H.; Kiran, P. P.; Rao, D. N. *Mater. Chem. Phys.* **2011**, *130*, 113–120.
- (9) Brow, R. K. *J. Non-Cryst. Solids* **2000**, *263*, 1–28.
- (10) Campbell, J. H.; Suratwala, T. J. *J. Non-Cryst. Solids* **2000**, *263&264*, 318–341.
- (11) Poirier, G.; Ottoboni, F. S.; Cassanjes, F. C.; Remonte, A.; Messaddeq, Y.; Ribeiro, S. J. L. *J. Phys. Chem. B* **2008**, *112*, 4481–4487.
- (12) Rani, S.; Sanghi, S. *J. Alloys Compd.* **2009**, *477*, 504–509.
- (13) Rothermel, J. J. *J. Am. Ceram. Soc.* **1949**, *32*, 286–289.
- (14) Al-Hawary, A. S. *J. Phys. Chem. Solids* **1997**, *58*, 1325–1328.
- (15) Chahine, A.; Et-Tabirou, M. *Mater. Res. Bull.* **2002**, *37*, 1973–1979.
- (16) Jiraik, J.; Koudelka, L.; Polspisil, J.; Montagne, L. *J. Mater. Sci.* **2007**, *42*, 8592–8596.
- (17) Montagne, L.; Palavit, G.; Mairesse, G. *Phys. Chem. Glasses* **1996**, *37*, 206–211.
- (18) Shaim, A.; Et-Tabirou, M.; Monatgne, L.; Palavit, G. *Phys. Chem. Glasses* **2002**, *37*, 245–249.
- (19) Poirier, G.; Messaddeq, Y.; Ribeiro, S. J. L.; Poulain, M. *J. Sol. State Chem.* **2005**, *178*, 1533–1538.
- (20) Dumbaugh, W. H.; Lapp, J. C. *J. Am. Ceram. Soc.* **1992**, *75*, 2315–2326.
- (21) Nasu, H.; Uchigaki, T.; Nakamura, M.; Kamiya, K.; Saka, S.; Soga, N. *Proc. Int. Conf. Sci. Technol. New Glasses* **1991**, 175–176.
- (22) Gomes, L. A.; de Araújo, C. B.; Messias, D. N.; Misoguti, L.; Zílio, S. C.; Nalin, M.; Messaddeq, Y. *J. Appl. Phys.* **2006**, *100*, 116105–116108.
- (23) Oliveira, T. R.; Fedus, K.; Manzani, D.; Falcão-Filho, E. L.; Boudebs, G.; de Araújo, C. B.; Messaddeq, Y. *J. Appl. Phys.* **2010**, *108*, 103523/1–103523–5.
- (24) Poirier, G.; de Araújo, C. B.; Messaddeq, Y. *J. Appl. Phys.* **2002**, *91*, 10221–10224.
- (25) Fedus, F.; Boudebs, G.; Coulombier, Q.; Troles, J.; Zhang, X. H. *J. Appl. Phys.* **2010**, *107*, 023108–023108/5.
- (26) Seo, Y. S.; Fujimoto, Y.; Nakatsuki, M. *Opt. Commun.* **2006**, *266*, 169–171.
- (27) Gomes, A. S. L.; Falcão-Filho, E. L.; de Araújo, C. B.; Rativa, D.; de Araujo, R. E.; Sakaguchi, K.; Mezzapesa, F. P. *J. Appl. Phys.* **2007**, *101*, 033115–033115/7.
- (28) Gopinath, J. T.; Shen, H. M.; Sotobayashi, H.; Ippen, E. P.; Hasegawa, T.; Nagashima, T.; Sugimoto, N. *Opt. Express* **2004**, *12*, 5697–5702.
- (29) Sheik-Bahae, M.; Said, A. A.; Wei, T. H.; Hagan, D. J.; van Stryland, E. W. *IEEE J. Quantum Electron.* **1990**, *26*, 760–769.
- (30) Fedus, K.; Boudebs, G.; de Araújo, C. B.; Cathelinaud, M.; Charpentier, F.; Nazabal, V. *Appl. Phys. Lett.* **2009**, *94*, 061122–061122/3.
- (31) Morgan, S. H.; Madruguer, R. H. *J. Am. Ceram. Soc.* **1990**, *73*, 753–756.
- (32) Stranford, G. T.; Condrate, R. A.; Cornilsen, B. C. *J. Mol. Struct.* **1981**, *73*, 223–234.
- (33) Charton, P.; Gengembre, L.; Armand, P. *J. Solid State Chem.* **2002**, *168*, 175–183.
- (34) Nalin, M.; Poirier, G.; Ribeiro, S. J. L.; Messaddeq, Y.; Cescato, L. *J. Non-Cryst. Solids* **2007**, *353*, 1592–1597.
- (35) Kharlamov, A. A.; Almeida, R. M.; Heo, H. *J. Non-Cryst. Solids* **1996**, *202*, 233–240.
- (36) Vivier, V. *Electrochim. Acta* **2001**, *46*, 907–914.
- (37) Milam, D. *Appl. Opt.* **1998**, *37*, 546–550.
- (38) Araujo, C. C.; Strojek, W.; Zhang, L.; Eckert, H.; Poirier, G.; Ribeiro, S. J. L. *J. Mat. Chem.* **2006**, *16*, 3277–3281.
- (39) Manzani, D.; Fernandes, R. G.; Messaddeq, Y.; Ribeiro, S. J. L.; Cassanjes, F. C.; Poirier, G. *Opt. Mater.* **2011**, *33*, 1862–1866.
- (40) Falcão-Filho, E. L.; de Araújo, C. B.; Bosco, C. A. C.; Acioli, L. H.; Poirier, G.; Messaddeq, Y.; Boudebs, G.; Poulain, M. *J. Appl. Phys.* **2004**, *96*, 2525–2530.
- (41) Stegeman, G. Y. *Nonlinear Optics of Organic Molecules and Polymers*; CRC Press: Boca Raton, FL, 2002.